A new polythiophene-driven coating method on inorganic INT/IF-WS2 nanomaterial surface

Journal:	*RSC Advances*
Manuscript ID	RA-ART-10-2015-021370.R1
Article Type:	Paper
Date Submitted by the Author:	16-Dec-2015
Complete List of Authors:	Raichman, Daniel; Bar Ilan University, Department of Chemistry, Nanomaterials Research Center, Institute of Nanotechnology & Advanced Materials Binyamini, Rina B.; Bar Ilan University, Department of Chemistry, Nanomaterials Research Center, Institute of Nanotechnology & Advanced Materials lellouche, jean paul; Bar Ilan University, Department of Chemistry, Nanomaterials Research Center, Institute of Nanotechnology & Advanced Materials
Subject area & keyword:	Nanomaterials - Materials < Materials

SCHOLARONE™
Manuscripts

A new polythiophene-driven coating method on inorganic INT/IF-WS$_2$ nanomaterial surface

D. Raichman*, R. Ben-Shabat Binyamini* and J.-P. Lellouche

Department of Chemistry, Nanomaterials Research Center, Institute of Nanotechnology & Advanced Materials, Bar-Ilan University, Ramat Gan 5290002, Israel

Jean-Paul.M.Lellouche@biu.ac.il

* These authors contributed equally to the paper

ABSTRACT

Inorganic nanotubes and fullerene nanoparticles of tungsten disulfide (INTs-WS$_2$ and IFs-WS$_2$, respectively) are practically inert, hindering their usefulness in both research and commercial applications. The covalent attachment of functional species onto the surface of INTs-WS$_2$ is a critical first step in realizing the potential that INTs-WS$_2$ offer for producing high performance materials, systems, and products. In our previous work, we developed a unique and versatile method for functionalizing carboxylic groups on the nanotubes' surface. In this current research, we have developed a functionalization method *via* the Vilsmeier-Haack reaction using 2, 2'-bisthiophene-4-carboxaldehyde and POCl$_3$ as chemically reactive reagents. These coatings should improve the electro-conductivity and mechanical properties of both INTs-WS$_2$ and IFs-WS$_2$ inorganic nanomaterials. Using a bithiophene linker allowed us to polymerize any substituted thiophene monomer such as 3,4-ethylenedioxythiophene (EDOT) and 3-thiophene acetic acid (TAA) among others.

KEYWORDS Tungsten disulfide, nanotubes, fullerenes, thiophene, silica, nanoparticles, interfacial chemistry

1. Introduction

Conducting organic polymers (COPs) have attracted immense attention owing to their excellent electrical properties, superior thermal stability, high surface area, good environmental stability, corrosion resistance, along with suitable strength and fracture toughness.[1] Therefore, COPs are promising candidates for fabricating outstanding scientific and technical materials in a variety of applications such as electrodes for super capacitors[2-4], light-weight batteries, solar cells, as well as molecular electronic devices and sensors.[5] Some of the well-known electrical COPs are polyaniline (PANI),[6-8] polypyrrole (PPy),[9] polythiophene (PTh), poly(*o*-phenylenediamine), poly(3,4-ethylenedioxythiophene) (PEDOT), poly(*p*-phenylene), and among others. Polymer-based composites are usually obtained through the dispersion of organic/inorganic nanoparticles in a polymer matrix.

Despite the significant amount of progress made towards producing high-performance fibers from polymer materials, determining their mechanical properties constitutes only a fraction of the expected theoretical values for these materials.[10] Several technological developments in recent years have been utilized to improve the high-performance properties of polymer-based fibers.

Commercial products, including functional sportswear (*e.g.*, golf gloves), inner wear, skin-care products, filters, and precision grinding cloths (*e.g.*, polishing cloths), which take advantage of these polyester nano-fibers, have been developed owing to the large surface area, high adsorption, good dispersion, and filtration characteristics that these thin fibers possess.[11, 12] The first polymer composites (*e.g.,* fiber glasses) revolutionized the boating industry, and later in the 1960s, the advent of carbon fibers ushered in many innovative technologies for producing polymer composites, which increased their application range in daily life. Since then, carbon-fiber-reinforced polymer composites (CFRP) have remained a major standard for polymer-based materials, particularly in high-performance applications.

The recognition of multi-wall carbon nanotubes (MWNTs) in 1991[13] and single-wall carbon nanotubes (SWNTs) in 1993[14] brought about a new influx of research in lightweight, high-performance reinforced polymers. In comparison with conventional carbon fibers, the Young's modulus and tensile strength of these tubular graphitic materials were found to be ~1 TPa[15-18] and ~10 to 150 GPa[19-22] respectively. Therefore, composites incorporating carbon nanotubes (CNTs) have received a great deal of attention in both academia and industry for their potential replacement of carbon fibers in polymer-based reinforced materials.

Several reviews have already focused on summarizing the property enhancement of polymers by CNTs.[23-30] CNTs have been heralded as a "game-changer" for producing next-generation high-performance materials that will greatly improve the properties of current CFRPs. However, one major hang-up has also been the cost of these materials at small-scale production levels.

Recently, inorganic nanomaterials such as tungsten disulfide nanotubes (INTs-WS_2) and molybdenum disulfide (MoS_2) nanoplatelets have been used as reinforcing agents to improve the mechanical and tribological properties of epoxy composites, electrospun poly(methyl methacrylate) fibers, and biodegradable poly(propylene fumarate) (PPF) nanocomposites.[31-33] INTs-WS_2 possess high mechanical properties (a Young's modulus of 150 GPa, a bending modulus of 217 GPa)[34-36] and functional groups (such as sulfide, oxysulfide, and defect hydroxylated species). In addition, they can be readily dispersed in organic solvents, polymers, epoxy polymer for example, and resins. Owing to these potential benefits, the efficacy of INTs-WS_2 as nanoscale fillers to improve the mechanical properties of biodegradable polymers used for bone tissue engineering, for example, should be investigated.

However, only few researchers have focused on the functionalization of dichalcogenide-based materials and fewer have succeeded in creating covalent bonds between the sulfide functionality of WS_2 NPs and organic materials. Importantly, we have successfully developed a functionalization method for INT-WS_2 that uses readily available materials and equipment to produce an acidic, covalently bound shell of polyCOOH functional groups.[37] In continuing this research, we have developed a new two-step coating method utilizing polythiophene derivatives using a Vilsmeier-Haack-like type of chemical reaction by reacting 2, 2'- bithiophene-5-carboxaldehyde with INTs-WS_2 and $POCl_3$ as the activating agent[38] (Scheme 1) to afford intermediate nucleophilized INT/IF WS_2-bithiophene composites.

2
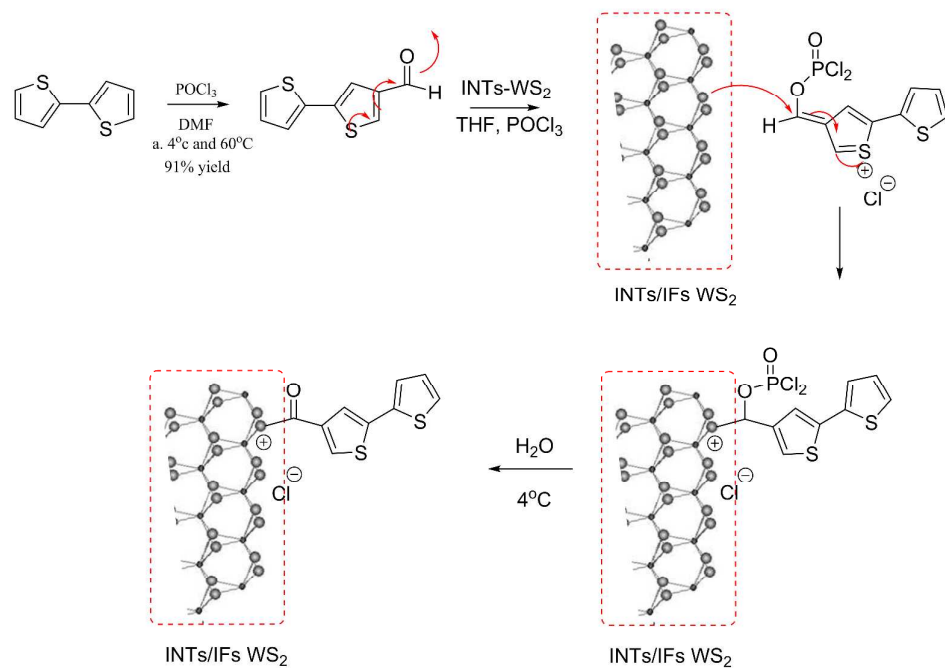
Scheme 1 Formation of INT/IF WS$_2$-bithiophene composites

Then, a 2nd step of liquid phase oxidative thiophene polymerization (Scheme 2) was carried out by using FeCl$_3$ as an oxidant agent and thiophene acetic acid (TAA) or 3,4-ethylenedioxythiophene (EDOT) as oxidizable thiophene monomers.
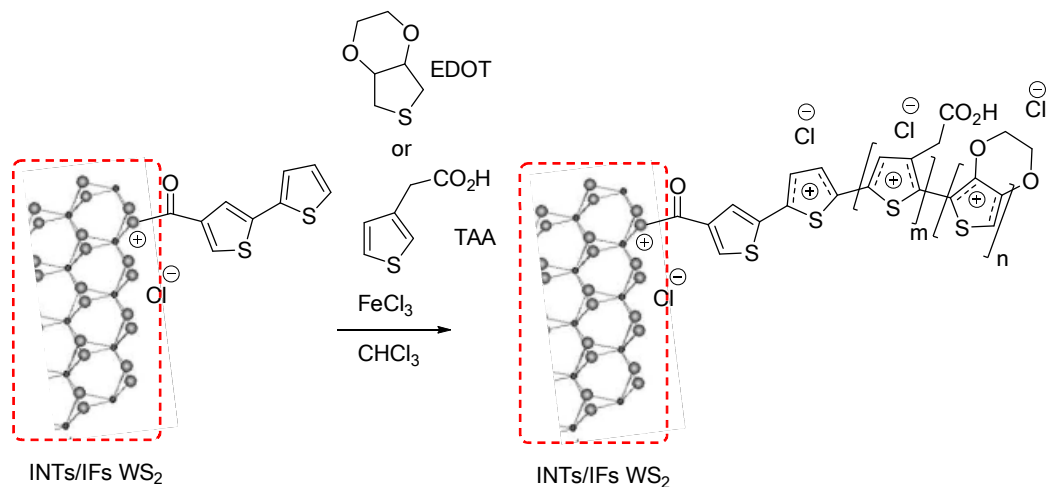
n or m = 0%, 25%, 50%, 75%, 100%

Scheme 2 2nd step oxidative polymerization of TAA/EDOT monomers onto the INT/IF WS$_2$-surface

2. Experimental

2.1. Materials

Tungsten disulfide inorganic nanotubes (INT-WS$_2$) and fullerenes (IFs-WS$_2$) were purchased from NanoMaterials Ltd (Yavne, Israel). All reagents and solvents were purchased from commercial sources and were used without further purification. Thermogravimetric analysis was performed on a TA Q600-0348, model SDT Q600 (Thermofinnigan) using a temperature profile of 25–800 °C at 10 °C/min under nitrogen flow (180 mL/min) with sample masses of 5-15 mg. IR spectra were recorded on an ATR id7 spectrometer (Thermo SCIENTIFIC). Nanomaterial surface charges were evaluated by ζ potential measurements with a Zetasizer Nano-ZS (Malvern Instruments Ltd., Worcestershire, UK) in water (pH unadjusted) at 25 °C and 150 V. Untreated and VH-treated INTs were characterized with a G2, FEI High-Resolution TEM (Tecnai). Dispersions of INT-WS$_2$ and f-INT-WS$_2$ were prepared with a low-power ElmaSonic S30 bath sonicator (Elma GmbH & Co., Singen, DE). The chemically accessible PTAA shell present on the surface of the polyCOOH f-INT-WS$_2$ was quantified by the Kaiser test after shell derivatization using 1,3-diaminopropane. HR-SEM microphotographs were acquired using an Extreme High-Resolution (XHR) FEI® MagellanTM 400 L scanning electron microscope. Samples were prepared by placing dried powder onto a copper plate. EPR measurements were performed with an X-band Elexsys E500 EPR spectrometer (Bruker, Karlsruhe, DE) with integrated frequency counter. A 3 mm ID quartz sample tube was used and placed at the ER 4122SH.Q cavity of the EPR. Recording parameters included microwave in a field of 3300-3500 Gauss. Measurements were performed on a Kratos AXIS-Ultra-DLD spectrometer, using a monochromatic Al ka source at 15-75 W and detection pass energies ranging between 20 to 80 eV. Base pressure in the chamber was below 10^{-9} torr. Sample charging was encountered at different levels, depending on the size of inspected grain. This artifact was addressed by means of an electron flood gun (eFG) and the comparison of data with and without eFG application.

Synthesis of 2,2'-bithiophene-5-carboxaldehyde

First, 1.103 g of 2,2'-bithiophene (6.65 mmol) was dissolved in 10 ml of DMF. The solution was cooled to 4°C in an ice bath and 650 μl of POCl$_3$ (6.93 mmol) were added dropwise. The solution was stirred at 4°C for 20 minutes and then heated to 60°C with overnight stirring. The solution was cooled to 4°C and 10 ml of water was added in order to neutralize the excess of POCl$_3$. The water/DMF solution was added to a separation funnel and to 20 ml of ethyl acetate. The organic phase was extracted with ethyl acetate (20 ml x 4 times) and recombined. Then, the organic phase was washed with water (20 ml x 10 times) to remove the DMF. The organic phase was dried over MgSO$_4$ and filtrated to a 200 ml round bottomed flask and evaporated to obtain 1.231 g of green solid (91.44% yield).

^{1}H-NMR (acetone-d^6) 300MHz

δ = 9.925 ppm, s, 1H. δ = 7.92 ppm, d, (J = 1.2Hz, 5.1Hz), 1H. δ = 7.615ppm, dd, (J = 1.2Hz, 3.6Hz), 1H. δ = 7.535 ppm, dd, (J = 1.2Hz, 3.6Hz) 1H, δ = 7.459 ppm, d, (J = 3.9Hz), 1H. δ =7.167 ppm, dd, (J = 3.6Hz, 5.1Hz), 1H.

^{13}C-NMR (acetone-d^6) 300MHz

δ = 183.7 ppm (C=O), δ = 139.021ppm (C-H), δ = 129.5 ppm (C-H), δ =128.429 ppm (C-H), δ = 127.281 ppm (C-H), δ= 125.564 ppm (C-H).

MS: *m/z* calculated for $C_9H_6OS_2$ 194 for M.

2.2. Synthesis of (2-thiophene-3-yl)-*N*-(3-(triethoxysilyl)propyl)acetamide)

3-Thiophene-acetic acid (1.4 g, 5.0 mmol), dissolved in a mixture of anhydrous 1,2-dichloro-ethane (20.0 mL) and anhydrous THF (20.0 mL), was added to 1,1'-carbonyldiimidazole (CDI, 1.94 g, 5.0 mmol, at 20°C), and the reaction mixture was stirred at room temperature for 2 h. Then, (3-aminopropyl)-triethoxysilane (APTES, 2.8 mL, 6.0 mmol) was added to the reaction mixture, which was stirred at room temperature for an additional 24 h. Next, when the reaction was completed (checked by TLC), the medium was concentrated in a vacuum and purified by flash chromatography on silica gel (eluent: *n*-hexane:ethyl acetate = 85: 15) to afford the pure oily colorless thiophene-based silicate (1.1 g, 3.18 mmol, 63%)

H^1-NMR (chloroform-d) 300 MHz

δ 7.31 (dt, *J* = 1, 8 Hz, 1H), 7.13 (s, 1H), 7.01 (ddd, *J* = 2, 6, 8 Hz), 3.77 (q, *J* = 7 Hz, 6H), 3.57 (s, 2H), 3.22 (q, *J* = 6 Hz, 2H), 1.59 (qv. *J* = 8 Hz, 2H), 1.18 (t, *J* = 7 Hz, 9H), 0.58 (t, *J* = 8 Hz, 2H) ppm; ^{13}C-NMR (CDCl$_3$ MHz): δ 171.6, 137.6, 127.9, 126.3, 121.2, 58.4, 43.5, 35.8, 25.2, 18.3, 13.8 ppm; FT-IR (KBr): 1078 (C-O) (s), 1534 (CONH$_2$) (s), 1647 (CON) (s), 2973 (CH$_2$) (s), 3342 (OH) (s). MS: *m/z* calculated for $C_{15}H_{27}NO_4SSi$ 345 for MH$^+$, found 346 and MNa$^+$, found 368.

2.4. Synthesis of 3'-(4-tert-butylphenyl)thiophene

First, 287 µl of 3-bromothiophene (3.067 mmol) was dissolved in 10 ml THF and 10 ml of K$_2$CO$_3$ 2M). Then, 1.092 g of 4-*tert*-butylphenylboronic acid (6.1348 mmol), 15mg of palladium acetylacetonate, and 30 mg of triphenyl phosphine were added to the mixture. The reaction mixture was refluxed under N$_2$ streaming overnight. The reaction was monitored with TLC (hexane 100%). The phases were separated in a separation funnel. The aqua phase was extracted with DCM. The organic phase was dried under MgSO$_4$ and evaporated to obtain yellow oil. The crude was purified in an alumina column (100% hexane) to obtain 620 mg (2.87 mmol) of white solid (93.6% yield).

H^1-NMR (acetone-d^6) 400MHz

δ = 7.48-7.66ppm, m, 7H. δ= 1.34ppm, s, 9H.

^{13}C-NMR (acetone-d^6) 400MHz

δ = 150.79 ppm (C), δ = 127.22 ppm (CH), 127.017 ppm (CH), δ = 126.85 ppm (CH), δ= 126.54 ppm (CH), δ = 120.65 ppm (CH). Δ = 113.40 ppm (C), δ = 108.43 ppm (C), δ = 31.65 ppm (CH$_3$).

2.5. Synthesis of INTs-WS$_2$-2,2' bithiophene

First, 300 mg of 2,2' bithiophene-5-carboxaldehyde (1.544 mmol) were dissolved in 30 ml THF and cooled to 4°C in an ice bath. Then, 400 µl of POCl$_3$ were added and stirred for 30 minutes. Next, 350 mg of INTs WS$_2$ were added and the dispersion was refluxed overnight. The dispersion was cooled to 4°C in an ice bath and 20 ml of water were added to neutralize the POCl$_3$ in excess. The dispersion was poured into centrifuge tubes and separated in centrifuge (8,000 rpm for 5 minutes). Next, it was washed with ethanol and centrifuged 5 times (5 minutes 8,000 rpm each rotation). Finally, it was dried in vacuum to obtain 280 mg of INTs-WS$_2$-2,2' bithiophene.

2.6. Synthesis of INTs-WS₂-bithiophene-polythiophene acetic acid

60 mg of INTs-WS₂-2,2' bithiophene were dispersed in 5 ml of chloroform and then 120 mg of FeCl₃ (0.74 mmol) were added and stirred for 30 minutes at room temperature. Then, 120 mg of thiophene acetic acid (0.84 mmol) were added and the suspension was stirred for 1 hour at room temperature. The suspension was poured into an eppendorf tube and centrifuged (5 minutes, 8,000 rpm). The INTs were washed with ethanol 5 times (5 minutes, 8,000 rpm) and dried in vacuum to obtain 55 mg of INTs-WS₂-bithiophene-polythiophene acetic acid.

2.7. Synthesis of INTs-WS₂-bithiophene-Polythiophene acetic acid / poly 3,4–ethylenedioxythiophene

60 mg of INTs-WS₂-2,2' bithiophene were dispersed in 5 ml of chloroform and 120 mg of FeCl₃ (0.74 mmol) and stirred for 30 minutes at room temperature. Then, 30 mg/60 mg/90 mg of thiophene acetic acid (0.21 mmol/0.42 mmol/0.633 mmol) and 90 mg/60 mg/30mg of 3,4-ethylenedioxythiophene (0.633 mmol/0.42 mmol/0.21 mmol), respectively, were added and stirred for 1 hour at room temperature. The suspension was poured into an eppendorf tube and centrifuged (5 minutes, 8,000 rpm). Next, the INTs were washed with ethanol 5 times (5 minutes, 8,000 rpm) and dried in vacuum to obtain 80-100 mg of INTs-WS₂-bithiophene-polythiophene acetic acid-poly-3,4-ethylenedioxythiophene.

2.8. Synthesis of INTs-WS₂-bithiophene-poly-3,4-ethylenedioxythiophene

60 mg of INTs-WS₂-2,2' bithiophene were dispersed in 5 ml of chloroform and 120 mg of FeCl₃ (0.74 mmol) and stirred for 30 minutes at room temperature. Then, 180 µl of 3,4-ethylenedioxythiophene (0.95 mmol) were added and stirred for 1 hour at room temperature. The suspension was poured into an eppendorf tube and centrifuged (5 minutes, 8,000 rpm). The INTs were washed with ethanol 5 times (5 minutes, 8,000 rpm) and dried in vacuum to obtain 80-100 mg of INTs-WS₂-bithiophene-poly-3,4-ethylenedioxythiophene.

2.9. Coupling of 1,3 diaminopropane to INTs-WS₂-Polythiophene acetic acid/poly 3,4-ethylenedioxythiophene

30 mg of INTs-WS₂-polythiophene acetic acid/poly 3,4-ethylenedioxythiophene (25%, 50%, 75%) were dispersed in 3 ml of chloroform and 200 mg of 1-ethyl-3-(3-dimethylaminopropyl) carbodiimide hydrochloride (1.57 mmol) and stirred for 30 minutes (room temperature). Then, 300 µl of 1,3 diaminopropane (3.6 mmol) were added and stirred overnight at room temperature. Next, the suspension was poured into an eppendorf tube and centrifuged (5 minutes, 8,000 rpm). Finally, the INTs were washed with ethanol 5 times (5 minutes, 8,000 rpm) and dried in vacuum to obtain 25-30 mg of INTs.

2.10. INTs-WS₂-polythiophene acetic acid/poly 3,4 ethylenedioxythiophene cleavage

50 mg of INTs WS₂ polythiophene acetic acid/poly 3,4-ethylenedioxythiophene were dispersed in 3 ml dichloromethane. Then, 1 ml of TFA was added and stirred for 1 hour at room temperature. The INTs were separated in a centrifuge and the supernatant was evaporated to obtain a purple/black solid.

3.0. Cleavage of the INTs/IFs-WS₂-Bithiophene/PTAA linker

30 mg of INTs/IFs-WS₂-bithiophene/PTAA were dispersed in 3 ml of HCl 0.01N / NH₄OH 0.01N and stirred for one day/ two days/ one week at room temperature. The nanotubes were separated and washed with water (x5) and ethanol (x5) in a centrifuge 10,000 rpm at 20°C for 5 minutes each rotation. The filtrate was kept for further

analysis. Next, the filtrate from above was extracted with ethyl acetate three times, 3 ml each time. Finally, it was dried over $MgSO_4$, filtrated, and evaporated to obtain oil.

3.1. Polymerization of 2-thiophene-3-yl-*N*-(3-(triethoxysilyl)propyl)acetamide) onto INTs/IFs-WS$_2$

25 mg of INTs/IFs-bithiophene, previously dispersed in an ultrasonic bath (Elmasonic S 30 ultrasonic bath, 37 kHz at full power irradiation) for 7 minutes, were placed in a reaction vessel containing 5 ml of H_2O. Then, 0.53 ml of ammonium hydroxide and 0.228 g (0.75 mmol, 11% molar) of 2-thiophene-3-yl-N-(3-(triethoxysilyl)propyl)acetamide) were added to the reaction vessel. The reaction was performed at room temperature for 24 h with constant agitation by an orbital shaker. The resulting suspension was washed with ethanol using a centrifuge for 10 min, 8,000 rpm, at 4^oC five times.

3.2 Polymerization of 2-thiophene-3-yl-*N*-(3-(triethoxysilyl)propyl)acetamide)-TEOS onto INTs/IFs-WS$_2$

25 mg of INTs/IFs-bithiophene, previously dispersed in ultrasonic bath (Elmasonic S 30 ultrasonic bath, 37 kHz at full power irradiation) for 7 minutes were placed in a reaction vessel containing 5 ml of H_2O. Then, 0.53 ml of ammonium hydroxide and 1.5 ml (6.72 mmol) of TEOS were added. The reaction was mixed for 3 minutes and then 0.228 g (0.75 mmol, 11% molar) of 2-thiophene-3-yl-N-(3-(triethoxysilyl)propyl)acetamide), which was previously dissolved in 1 ml ethanol, was added to the reaction vessel. The reaction was performed at room temperature for 24 h with constant agitation by an orbital shaker. The resulting suspension was washed with ethanol using a centrifuge for 10 min, 8,000rpm, at 4^oC five times.

3.2. Co-polymerization of 3'-(4'-tert-butyl-benzene)-thiophene-TEOS onto INTs/IFs-WS$_2$

25 mg of INTs/IFs-bithiophene, previously dispersed in ultrasonic bath (Elmasonic S 30 ultrasonic bath, 37 kHz at full power irradiation) for 7 minutes were placed in a reaction vessel containing 5 ml of H_2O. Then, 0.53 ml of ammonium hydroxide and 1.5 ml (6.72 mmol) of TEOS was added. The reaction was mixed for 3 minutes and then 0.228 g (0.75 mmol, 11% molar) of 2-thiophene-3-yl-*N*-(3-(triethoxysilyl)propyl)acetamide), which was previously dissolved in 1 ml ethanol, was added to the reaction vessel. The reaction was performed at room temperature for 24 h with constant agitation by an orbital shaker. The resulting suspension was washed with ethanol using a centrifuge for 10 min, at 8,000rpm, at 4^oC five times.

3.3. Polymerization of INTs-WS$_2$-poly-3'-bromothiophene

200 mg of INTs-WS$_2$-bithiophene were dispersed in 10 ml of chloroform and 400 mg of $FeCl_3$ and stirred for 30 min at room temperature. Then, a solution of 300 μl of 3'-bromothiophene (3.2 mmol) in 2 ml of chloroform was added dropwise and stirred for another hour. Next, the INTs were separated and washed with ethanol in a centrifuge (9,000 rpm, x 10 times, 5 min each rotation). Finally, they were dried under vacuum to obtain 212 mg of INTs-WS$_2$-poly-3'-bromothiophene.

3.4. Suzuki coupling on INTs-WS$_2$-poly 3'-(4-tert butylphenyl)-thiophene

100 mg of INTs-WS$_2$-poly-3'-bromothiophene was dispersed in a round bottomed flask with 10 ml THF and 10 ml 2M K_2CO_3. Then 472 mg of 4-tertbutyl-phenyl boronic acid (2.65 mmol), 10 mg of palladium acetyl acetonate, and 60 mg of triphenyl phosphine were added. The mixture was refluxed overnight. Next, the INTs were separated and washed with ethanol in a centrifuge (9,000 rpm, 10 times, 5 minutes for each rotation). Finally, they were dried under vacuum to obtain 92 mg of INTs-WS$_2$-poly 3'-(4-tert butylphenyl)-thiophene.

3.5. 1,3-diaminopropane coupling onto INTs-PTAA

30 mg of INTs-PTAA (or each copolymer) were dispersed in a solution of 150 mg of EDC•HCl (0.78 mmol) in 4 ml of DCM and stirred for 30 minutes. Then, 200 μl of 1,3-diaminopropane (3 mmol) were added and stirred overnight. Next, the nanotubes were separated in a centrifuge and washed with water 5 times and then with ethanol 3 times. Finally, they were dried under vacuum to obtain 23 mg of nanotubes.

Results and discussion

INTs-WS$_2$ and IFs-WS$_2$ NPs were functionalized with a shell of bithiophene followed by an additional shell of polythiophene oxidative polymerization derivatives (EDOT, TAA and a mixture of EDOT/TAA) using FeCl$_3$ as an oxidant agent. In order to quantify the amount of polymer coating on the WS$_2$ surface following UV-tracked washing steps (see Figure SI-3, Supplementary Information section for details), several tests were performed, including TGA, the Kaiser Test (after coupling 1, 3-diaminopropane onto the WS$_2$-bithiophene-PTAA) and quality tests such as FTIR, Raman, TEM, SEM, elemental analysis (EA), and EPR.

From the Raman shifts (514 nm laser excitation), we can learn about the presence of polythiophene acetic acid (PTAA) on the INTs/IF-WS$_2$ surface (Figure 1). The Raman spectrum is dominated by the first-order modes: $E^1_{2g}(\Gamma)$ at 349 cm^{-1} and $A_{1g}(\Gamma)$ at 418 cm^{-1}, which refers to the S-W-S band. Furthermore, peaks at 2953 cm^{-1} and 1473 cm^{-1} refer to C-H stretch and bend, respectively, thus confirming the presence of PTAA.
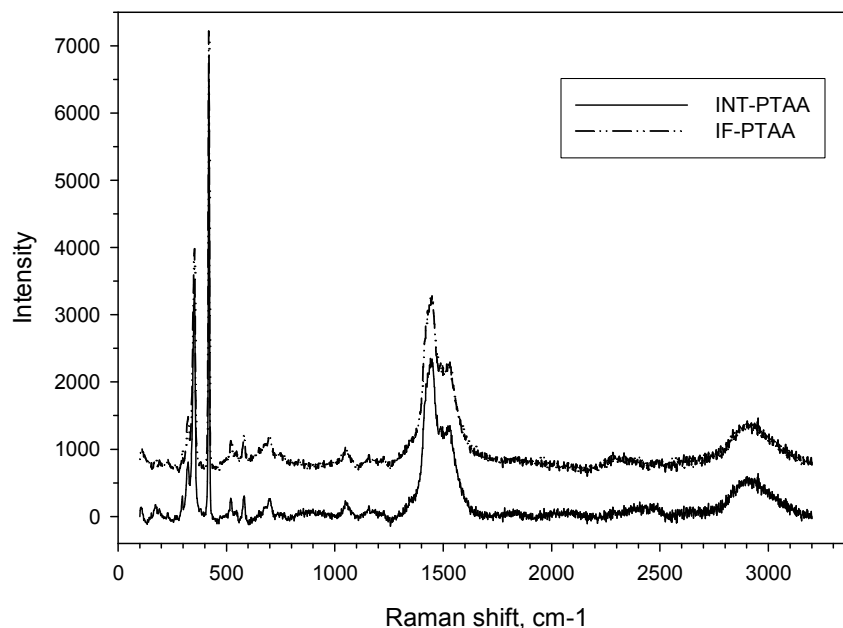
Figure 1 *Raman spectra of INTs/IF-WS$_2$-PTAA*

In order to confirm the presence of carbon on INTs/IF WS$_2$-PTAA/PEDOT, elemental analysis was carried out. The elemental analysis (chart 1) of INT-bithiophene shows 1.1% C and 0.1% of H, whereas after the attachment of PTAA, the carbon content rose to 6% and the H content to 0.4%. The increase in the C and H elements is due to the polymerization of the thiophene acetic acid. Examining INT-PTAA, INT-PTAA$_{25}$ PEDOT$_{75}$, INT-PTAA$_{50}$ PEDOT$_{50}$ 1M, and INT-PTAA$_{75}$ PEDOT$_{25}$, we found a correlation between the elevation in the C and H content and the

elevation in the co-polymer with the maximal PEDOT content. For instance, polymerization of 100% PTAA leads to 6% C and 0.4% H, whereas the polymerization of 25% PTAA/75% PEDOT leads to 29.8% C and 2.2% H. From the elemental analysis results, we can deduce that the electronically enriched EDOT monomer is more preferable since it polymerizes faster than does the TAA monomer.
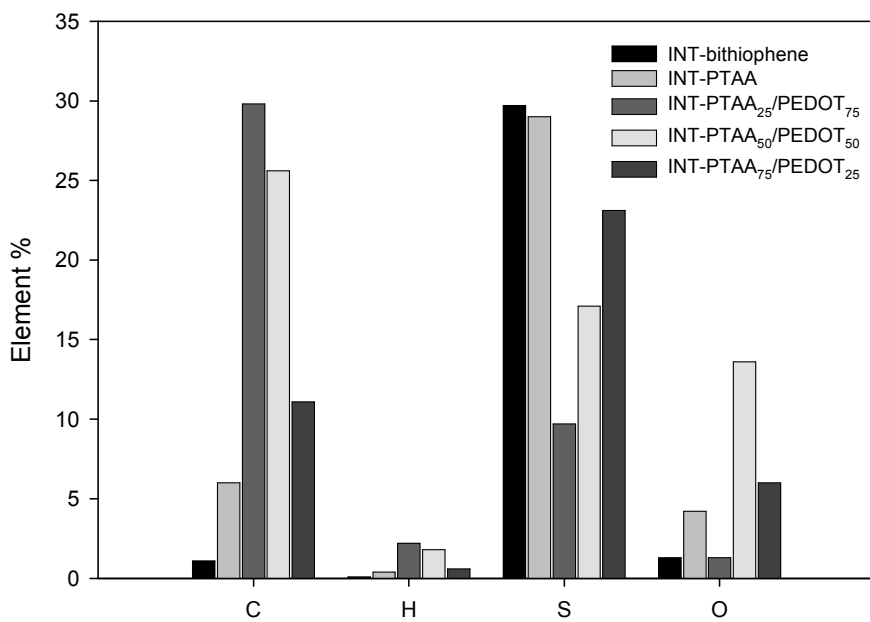

Chart 1 Elemental analysis of INTs-WS$_2$-PTAA/PEDOT

The elemental analysis of WS$_2$ fullerene is similar to the analysis of the WS$_2$ nanotubes. The C content, 0.74%, 31.8%, and the H content, 0.11%, 2.4% of IF-bithiophene and IF-PTAA 25%/PEDOT 75%, respectively (Chart 2) confirm our results about the INTs-polymers.
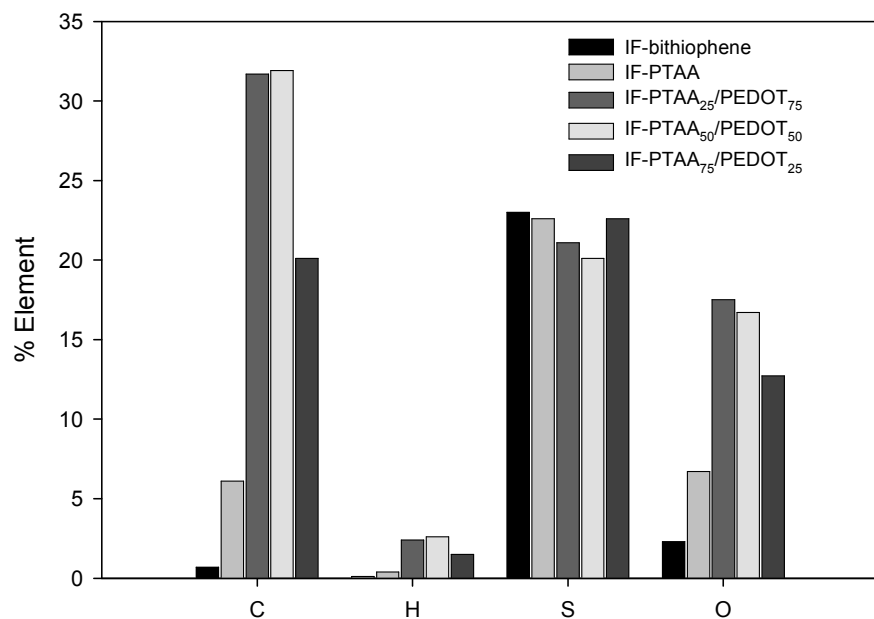
Chart 2 Elemental analysis of IF-WS$_2$-PTAA/PEDOT

The ESEM analysis (Figure 2) shows very nicely the polymer coating on the nanotube' s surface.

Figure 2 ESEM images of INTs-WS$_2$-bithiophene-PTAA

ESEM images of PTAA polymerized onto the surface of INT-bithiophene. The coating is uniform along the inorganic nanotubes and there is no evidence of polymerization of the PTAA outside the INTs.
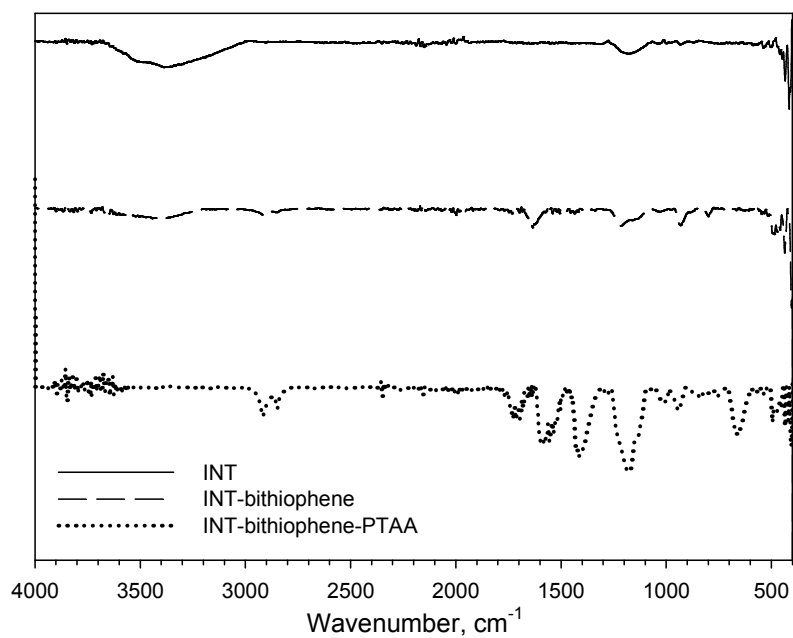
Figure 3 ATR spectra of INTs-WS$_2$, INTs-WS$_2$-bithiophene, & INTs-WS$_2$-PTAA

ATR-IR spectroscopy was used to confirm the presence of characteristic absorptions of the chemically modified f-INTs/IFs-WS$_2$ (Figures 3 and 4). Figures 3 and 4 display stacked spectra of the untreated samples and the two functionalized samples. The spectrum of unmodified INTs-WS$_2$ is nearly featureless, whereas the other two spectra exhibit characteristic peaks that indicate the presence of bithiophene and polythiophene acetic acid, respectively. The significant peaks can be assigned as follows: 1720cm^{-1} to 1610cm^{-1}, C=O of carboxylic acid and thioester, respectively; 2940 cm^{-1} and 1210 cm^{-1} to 1590 cm^{-1}, 670 cm^{-1} C-H stretch , C-H bend, and C-H "oop" bending (aromatic), respectively.
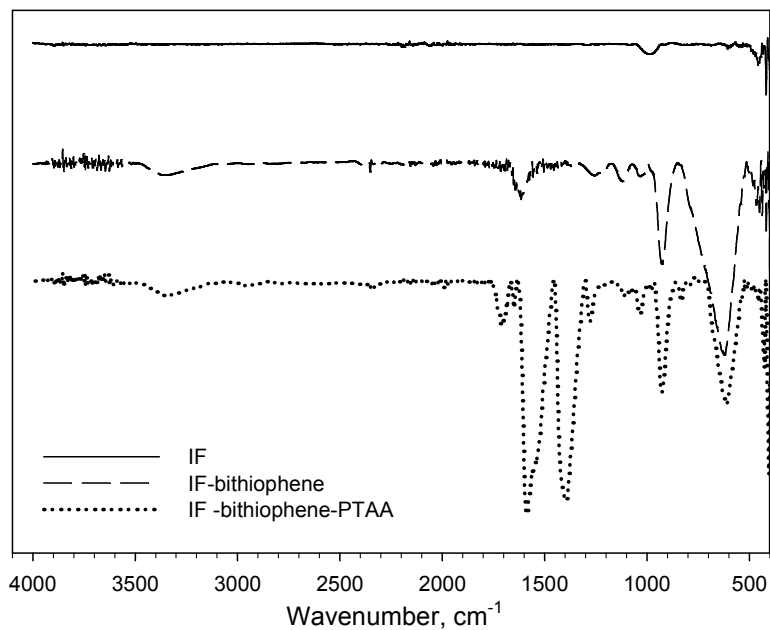
Figure 4 ATR spectra of IFs-WS$_2$, IFs-WS$_2$-bithiophene, & IFs-WS$_2$-PTAA composites

The ATR-IR spectra in Figure 4 (IFs) show results similar to those mentioned above for the INTs. The significant peaks can be assigned as follows: 1760 cm^{-1} to 1620 cm^{-1}, C=O of carboxylic acid and thioester, respectively; 3360 cm^{-1} , O-H stretch, 2910cm^{-1}, 1635cm^{-1} to 1390 cm^{-1}, 610 cm^{-1} C-H stretch , C-H bend, and C-H "oop" bending (aromatic), respectively.
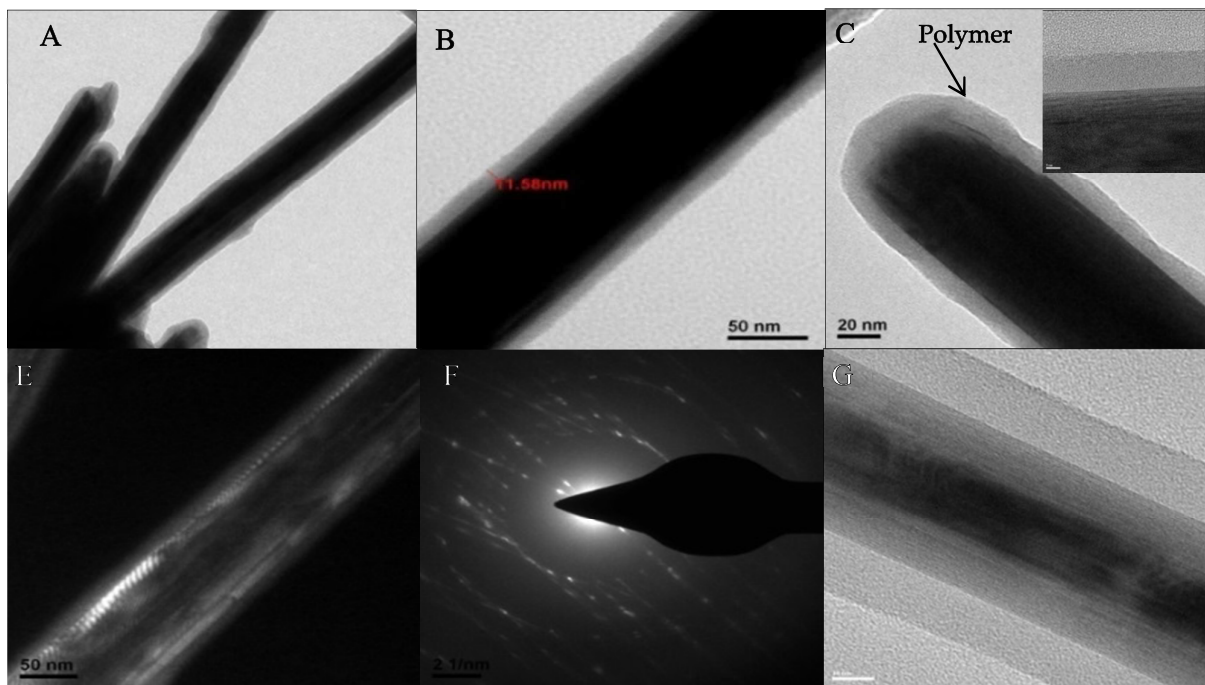
Figure 5 HR-TEM analysis of INTs-WS$_2$-PTAA

TEM images (Figures 5A-G) reveal a uniform poly-thiophene acetic acid coating approximately 10 nm thick. The dark field analysis (Figure 5 E) confirms that the coating is actually a different layer rather than an exfoliation of the INT since we did not note the non-crystalline coating at all. The diffraction analysis shows a crystalline structure that derives from the tungsten disulfide nanotubes, whereas the polymer has no crystalline structure at all.
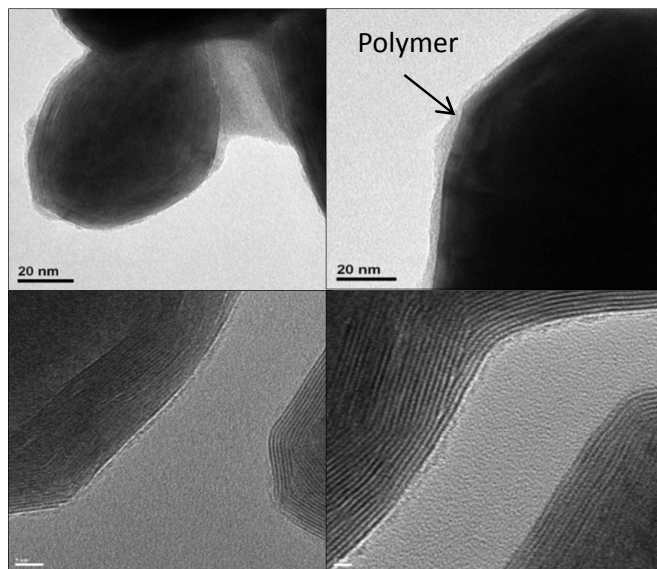

Figure 6 HR-TEM images of IFs-WS$_2$-PTAA

The TEM images of IFs-WS$_2$-PTAA (Figure 6) show a polymer coating on the inorganic fullerenes as well. Figures 6D and 6E were taken by higher magnification, which enabled us to distinguish the coating from the fullerene, and the organic polymer *vs.* the S-W-S layers. The polymer coating width is uniform and 5 nm thick, and the coating onto the INTs, under the same conditions, was thicker (11 nm). This may derive from the fact that the polythiophene is polymerized linearly whereas the fullerene has its own special bended shape that hinders polymer growth.
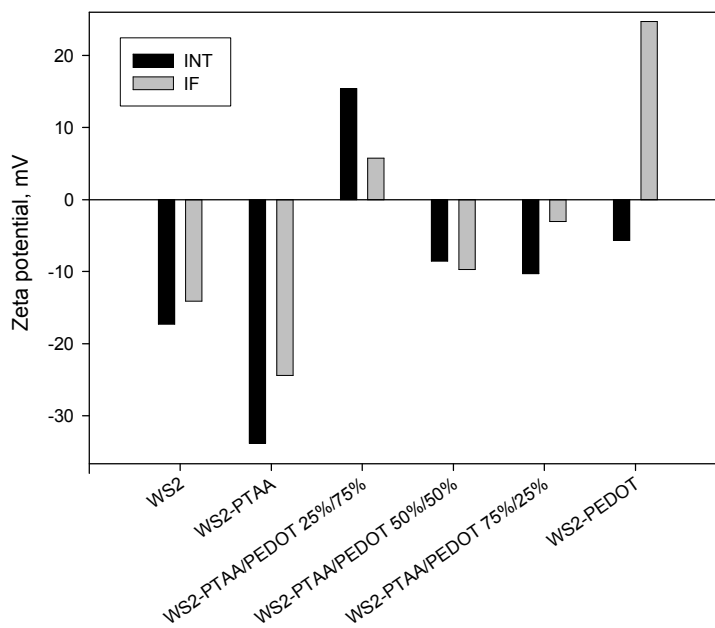
Chart 3 *Zeta potential of WS$_2$ before and after polymerization*

The Zeta potential analysis (Table 1) reveals that the polymer composites affect both charges of the tungsten disulfide nanotubes as well as of fullerene nanoparticles. As expected, polythiophene acetic acid transforms the INTs WS$_2$ charge to -33.8 mV after polymerization from -17.3 mV before polymerization. Moreover, as the concentration of PEDOT increases, the INTs WS$_2$ charge turns positive (+15.67 mV). The same correlation occurs with IFs WS$_2$ before and after polymerization. The Zeta potential of IFs WS$_2$ is -14.1 mV, whereas after PTAA coating, the Zeta potential changes to -24.4 mV. Nonetheless, while coating with PEDOT, the charge became positive +24.7 mV. By varying the concentration polymers (PTAA/PEDOT), different charges were obtained. If the PTAA concentration dominates the WS$_2$ surface, the charge will be more negative and vice versa, when the PEDOT monomer dominates, the charge will be more positive. These results confirm that WS$_2$ (IFs and INTs) are coated with the corresponding polythiophene polymer. These findings strengthen the elemental analysis results about the preference of the oxidative polymerization of EDOT over TAA onto both INTs and IFs.

In order to quantify the amount of thiophene acetic acid monomers on the WS$_2$-PTAA/PEDOT composites, 1,3-diaminopropane was coupled using EDC as a coupling agent. After deducing that all the carboxylic acid (which derives from TAA species) groups reacted with 1,3-diaminopropane (Scheme 3), a UV-sensitive Kaiser test was performed.
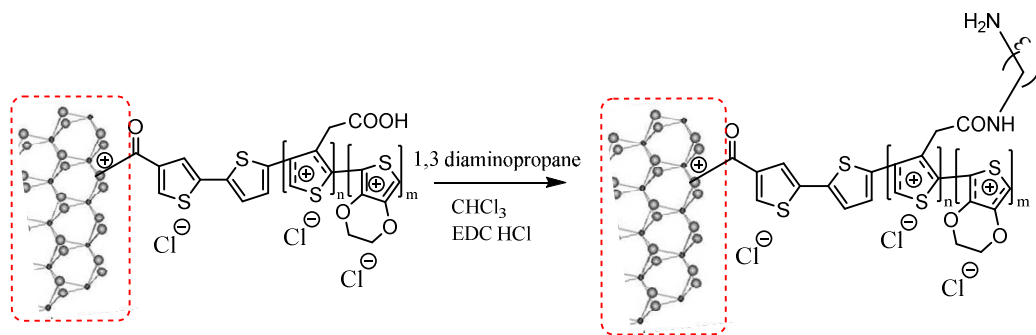
Scheme 3 1,3-diaminopropane coupling

The INTs-WS$_2$-PTAA and INTs-WS$_2$-PTAA/PEDOT (50% and 75% molar PTAA, respectively) composites yielded approximately the same results: 0.2180 mmol/g, 0.2110 mmol/g, and 0.2178 mmol/g, respectively, whereas the composite of INTs-WS$_2$-PTAA/PEDOT 25% molar INTs-PTAA contained only 0.1095 mmol/g. These results make sense since less carboxylic acid groups are available to react with 1,3-diaminopropane.

Table 1 Kaiser Test results

| Composite	Kaiser Values
INTs-WS$_2$-PTAA	0.2180 mmol/g
INTs-WS$_2$-PTAA$_{25}$/PEDOT$_{75}$	0.1095 mmol/g
INTs-WS$_2$-PTAA$_{50}$/PEDOT$_{50}$	0.2110 mmol/g
INTs-WS$_2$-PTAA$_{75}$/PEDOT$_{25}$	0.2178 mmol/g
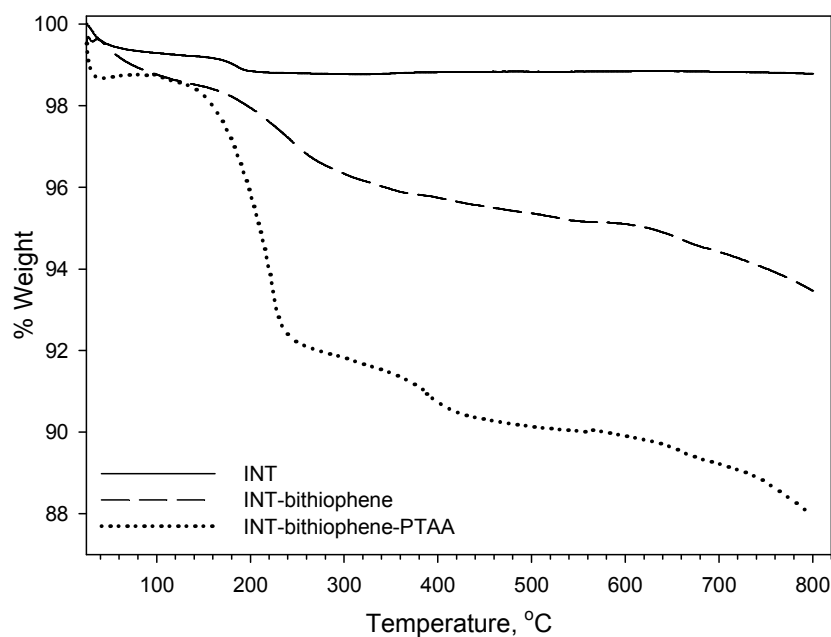
Figure 7 TGA curves of WS$_2$ INTs *vs.* WS$_2$-bithiophene and WS$_2$-PTAA

The TGA analysis reveals significant weight reductions of organic material for both WS$_2$-bithiophene and WS$_2$-PTAA (5.7% and 11.8%, repectively). The starting WS$_2$-INTs graph, on the other hand, shows a quite negligible reduction of 0.7% weight. Thus, these TGA results reinforce our previous results. The chemical stability of the decorating organic layer onto the WS$_2$ nanomaterial surface was also examined using TGA analysis. Functional INT-WS$_2$ bithiophene linker were incubated for 1 hour in an acidic aqueous 0.01N HCl (pH 4) solution, mimicking liquid phase polymerization conditions and its acidity generation (see Figure SI. 1, Supplementary Information section). Corresponding TGA graphs of the ***HCl-treated*** composite *vs.* the ***starting*** functional polyCOOH one disclose a very little difference in weight losses for the indicated 350-650°C temperature range of measurements, *i.e.,* ~1.06% (7.08-6.02 = 1.06%). These data clearly prove that the 2nd step polythiophene polymerization/growth from the WS$_2$-INT surface is fullly compatible with the significantly stable decorating organic shell.
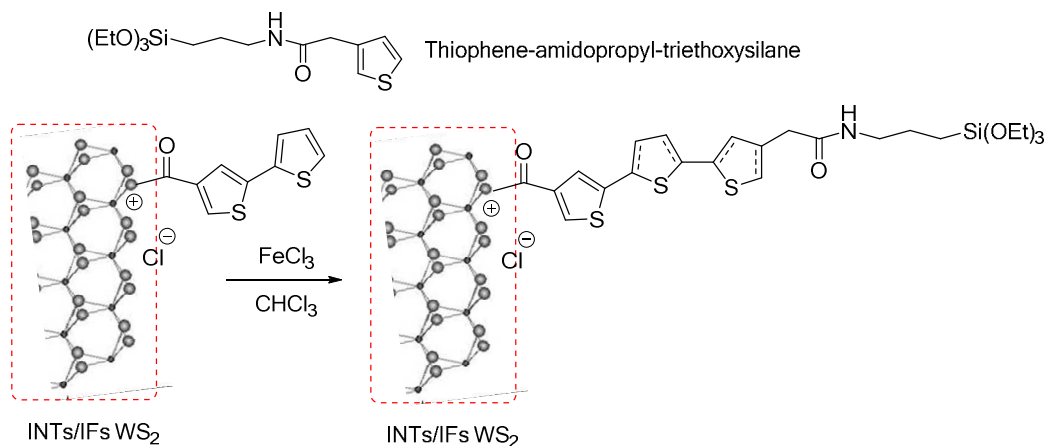
In order to test the variability of the polymerization, *thiophene-aminopropyl-triethoxysilane* was synthesized[35] and similarly oxidatively polymerized onto the same INTs-WS$_2$-bithiophene surface.

Interestingly, HR-SEM images (Figure 8) of the INTs-WS$_2$-polythiophene-aminopropyl-triethoxysilane composite show a nice coating of the polymer on the nanotube surface. This result indicates that the polymer is bonded covalently onto the tungsten disulfide nanotube surface.
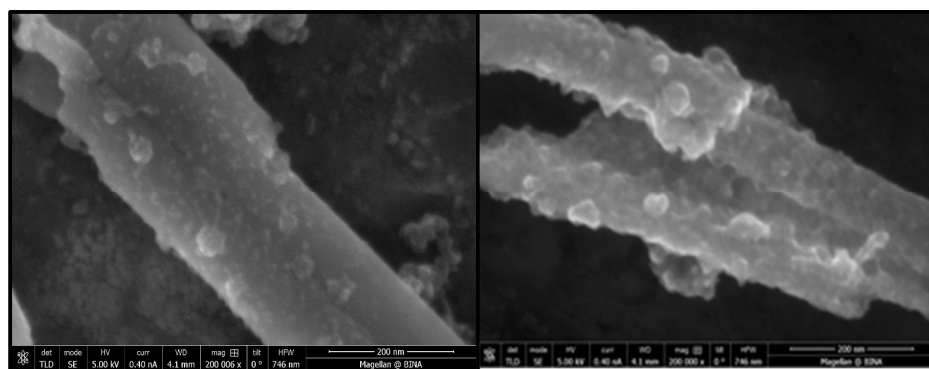

**Figure 8** HR-SEM microphotographs of the INTs-WS$_2$-Polythiophene-amidopropyl-triethoxysilane composite

2-(thiophene-3-yl)-N-(3-(triethoxysilyl)propyl)acetamide
INT-2-(thiophene-3-yl)-N-(3-(triethoxysilyl)propyl)acetamide

Wavenumber, cm^{-1}
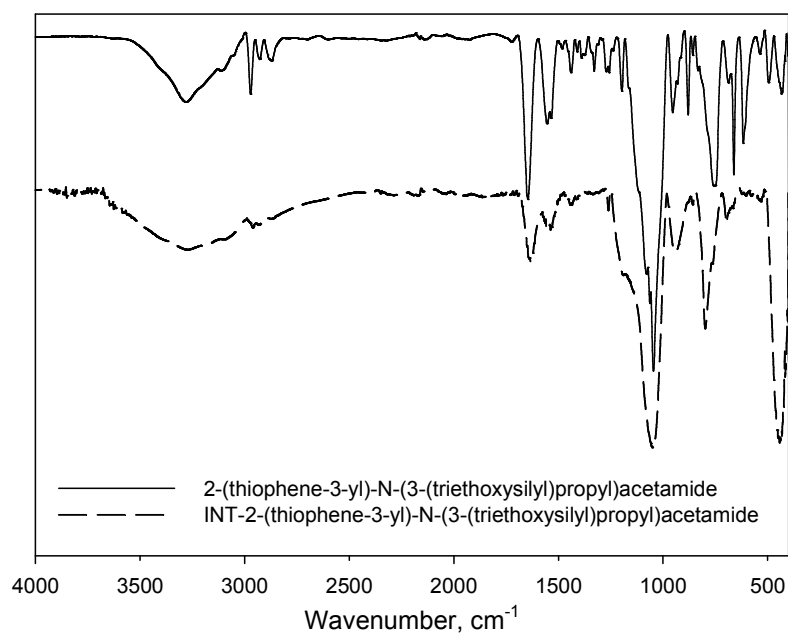
Figure 9 ATR spectra of INT-2-thiophene-3-yl)-*N*-(3-(triethoxysilyl)propyl)acetamide ***with*** and ***without*** Si NPs

The IR spectra of INTs-poly-*2-thiophene-3-yl)-N-(3-(triethoxysilyl)propyl)-acetamide* shows peaks at 1000 cm^{-1}-1070 cm^{-1}, which refers to Si-O stretchings. In addition, the peak at 1630 cm^{-1} belongs to the C=O stretch of the amide bond. The co-polymer with the Si NPs spectra shows the Si-O peak at 1030 cm^{-1}, which confirms the presence of a silica nanoparticulate phase on the nanotube surface. These results confirm the corresponding successful oxidative polymerization of the thiophene-silicate moiety onto these nanotubes.
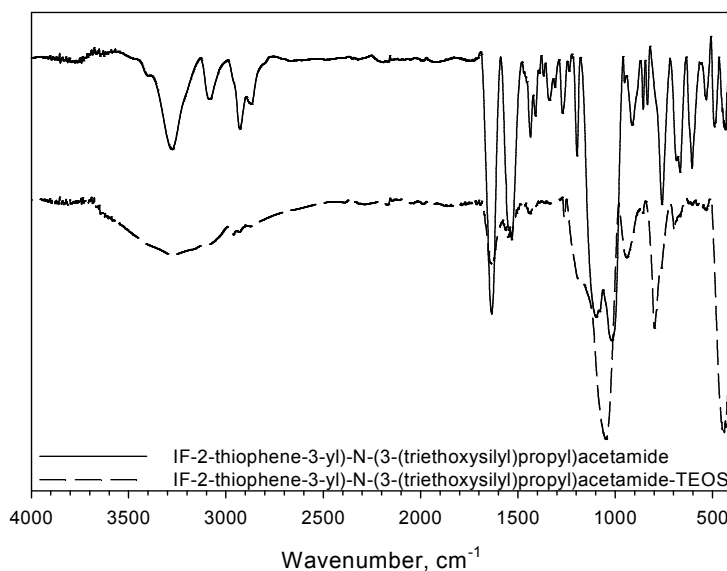
Figure 10 ATR spectra of IF-WS$_2$-poly 2-thiophene-3-yl)-*N*-(3-triethoxysilyl)propyl)acetamide *with* and *without* Si NPs

Same results (as mentioned above) have been also obtained onto the inorganic fullerene NP surface. The polymers were coated onto IF NPs (1670 cm^{-1} C=O, 2920 cm^{-1} C-H, 1050 cm^{-1} Si-O) and the silica nanoparticles also were successfully coated as well (1000 cm^{-1}-1100 cm^{-1} Si-O, and 3300 cm^{-1} O-H).

TGA spectra of INTs-poly 2-thiophene-3-yl)-*N*-(3-(triethoxysilyl)propyl)acetamide (Figure 11) without Si NPs show a weight loss of 41%. When one synthesized Si NPs *in situ*, the polymerization lead to an only 32% weight loss according to TGA analysis. The same correlation occurred with the IF-copolymer composite. Possibly, Si NP synthesis interferes with the thiophene polymerization and that is why less polythiophene-based organic material has been obtained.
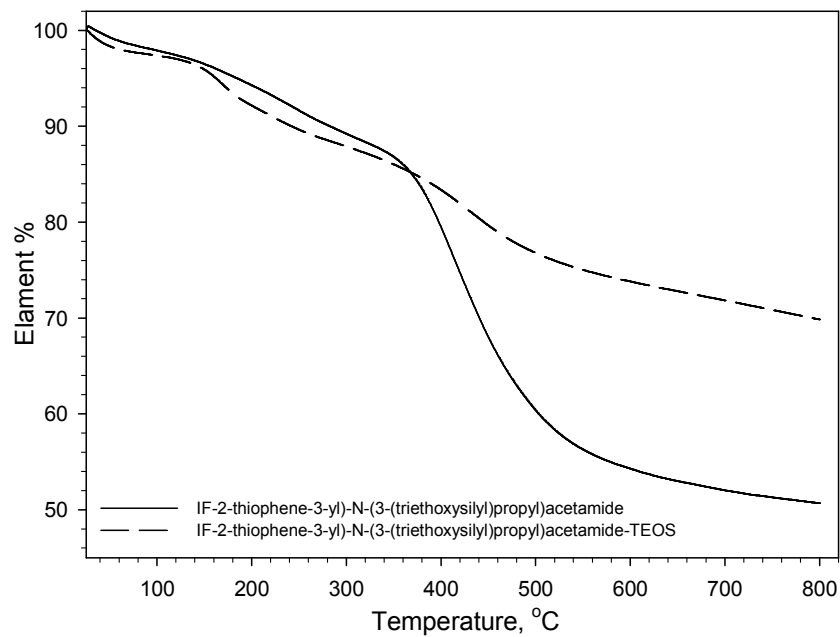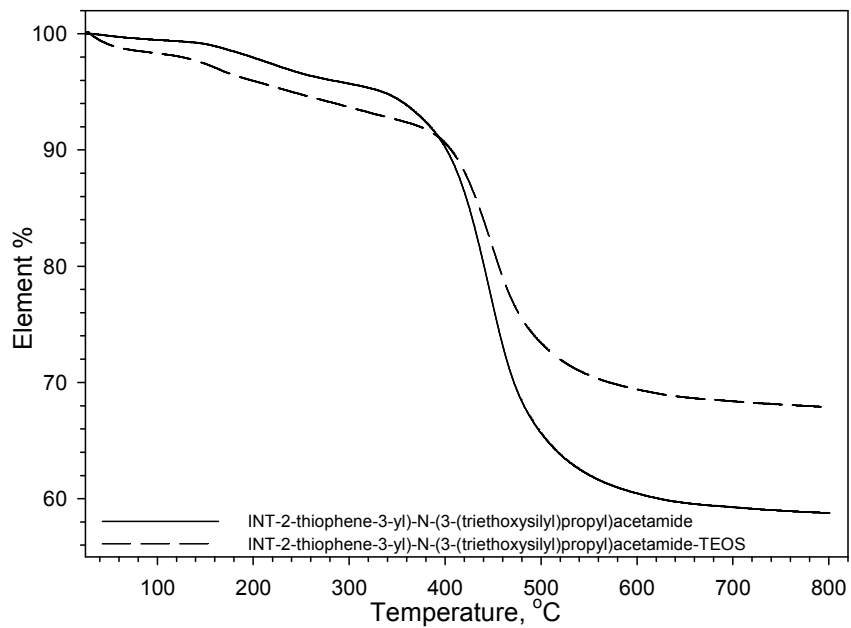
Figure 11 TGA spectra of poly 2-thiophene-3-yl)-*N*-(3-(triethoxysilyl)propyl)acetamide *with* and *without* Si NPs

Steric influence test
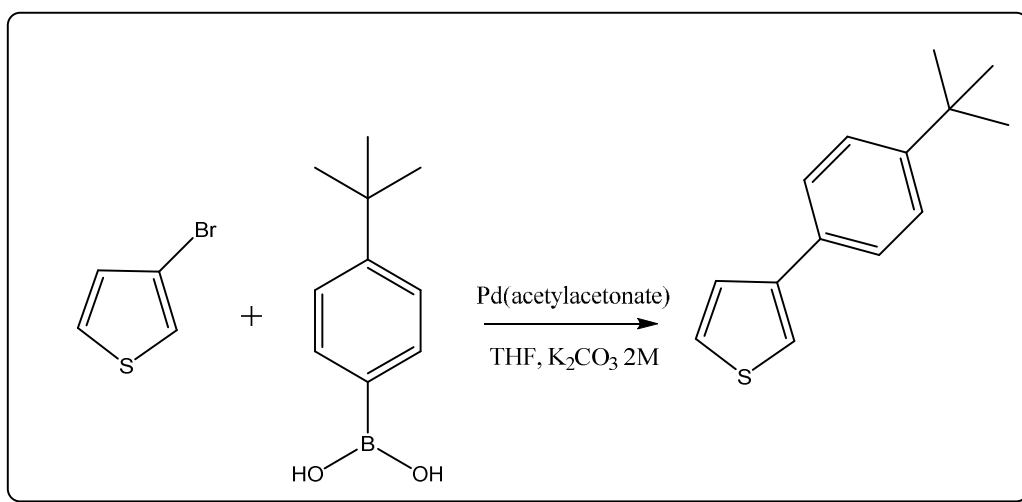
Scheme 5 Synthesis of 3'-(4-tert-butylphenyl)thiophene

It has been also interesting to determine the effect of more bulky thiophene-based monomers on the polymerization yield/effectiveness. To this end, the 3'-(4-*tert*-butylphenyl)-thiophene monomer was synthesized by using a well-known Suzuki coupling reaction. Thus, the oxidative polymerization using the former nucleophilized INTs-WS$_2$-bithiophene nanomaterial (scheme 6) was carried out (under the same conditions as mentioned above). Full analysis data can be found in the supporting information.
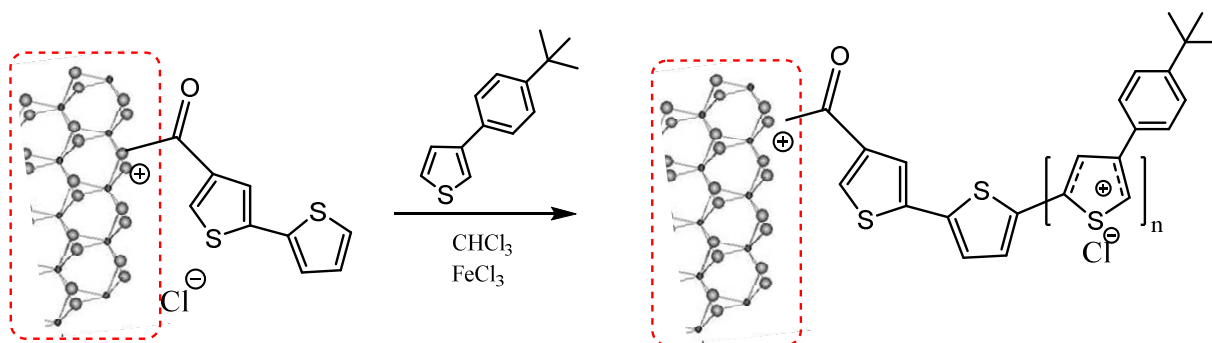
Method A

Scheme 6 Polymerization of 3'-(4'-tert-butyl- phenyl)-thiophene onto INTs-WS$_2$

TGA spectra of INTs-WS$_2$-poly-3'-(4-tert-butyl phenyl)-thiophene show two main reduction points, 251°C-478°C and 478°C-625°C, which refer to the polymer units. The nanotubes contain 6.85% of polymer according to the TGA results, whereas INTs-WS$_2$-bithiophene contains 3% of organic material (not counting the solvents/water evaporation).
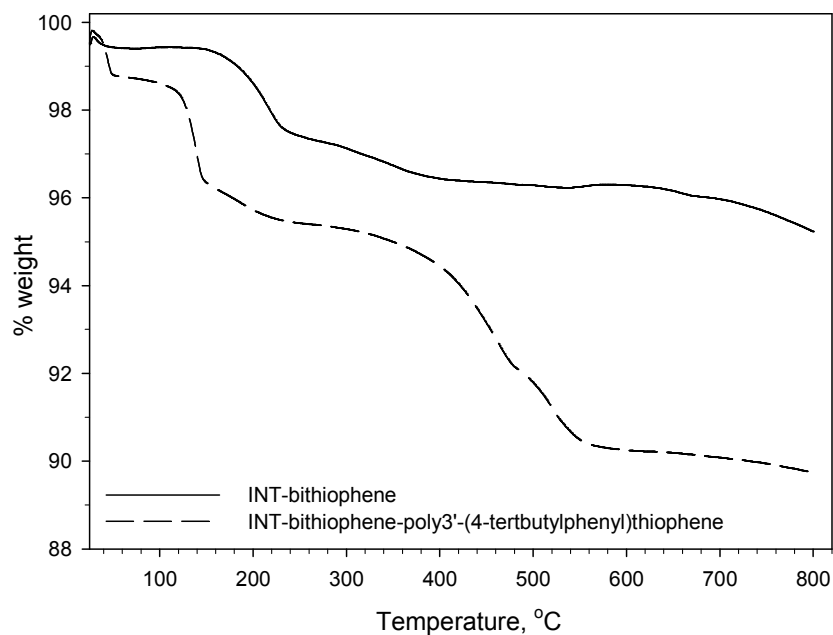
Figure 12 TGA spectra of INTs-WS$_2$-bithiophene *vs.* INTs-WS$_2$ poly-3'-(4-tert-butyl- phenyl)-thiophene

The Raman spectra confirm the presence of polymer on the INTs. The 2925 cm^{-1} and 1456 cm^{-1} peaks refer to C-H stretches and bends, respectively.
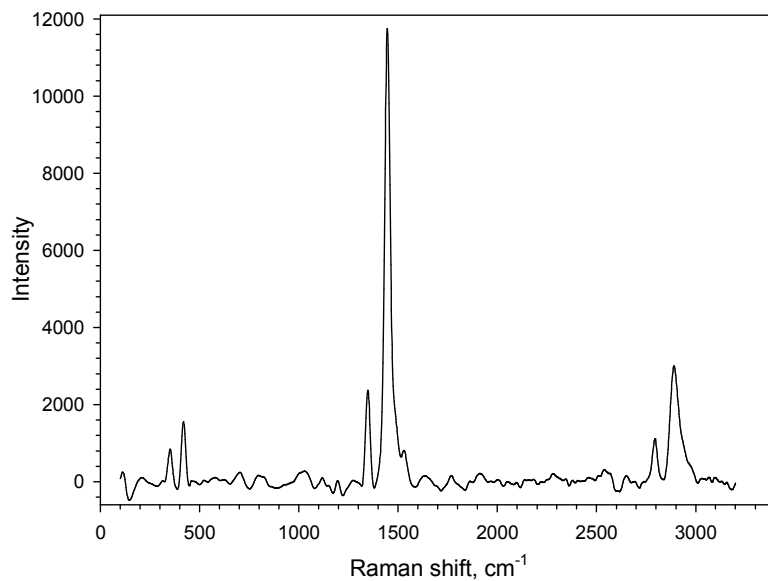

Figure 13 Raman spectra of INTs-WS$_2$-poly-3'-(4-tert-butyl-phenyl)-thiophene

In order to determine the effect of a bulky thiophene monomer on the polymerization yield/effectiveness, one decided to polymerize first the 3'-bromothiophene monomer and then perform a Suzuki coupling reaction using 4-tert-butylphenylboronic acid (Scheme 7).
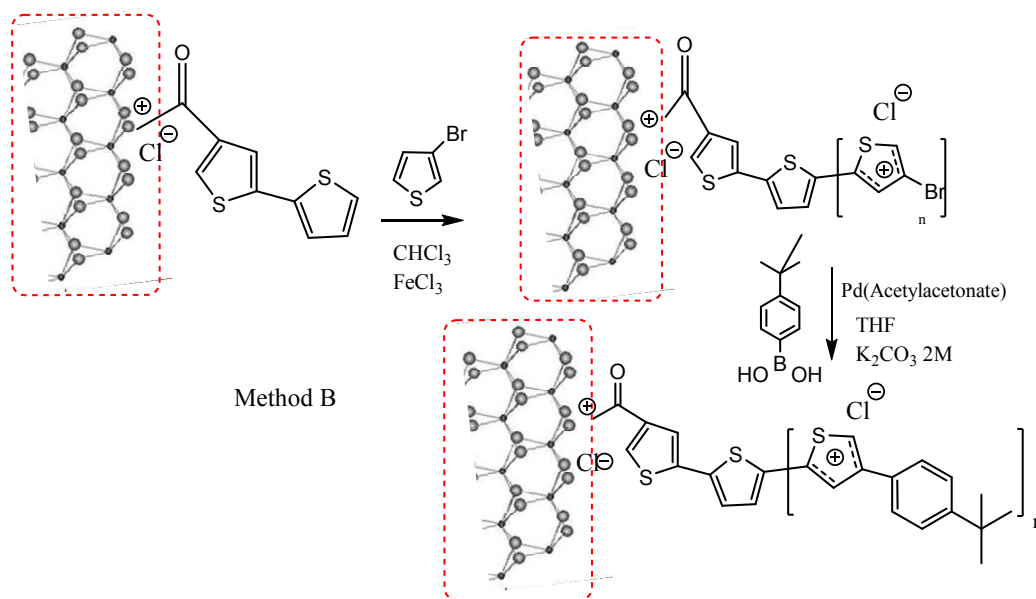
**Scheme 7** Two-step polymerization of 3'-(4'-tert-butyl-phenyl)-thiophene onto INTs-WS$_2$
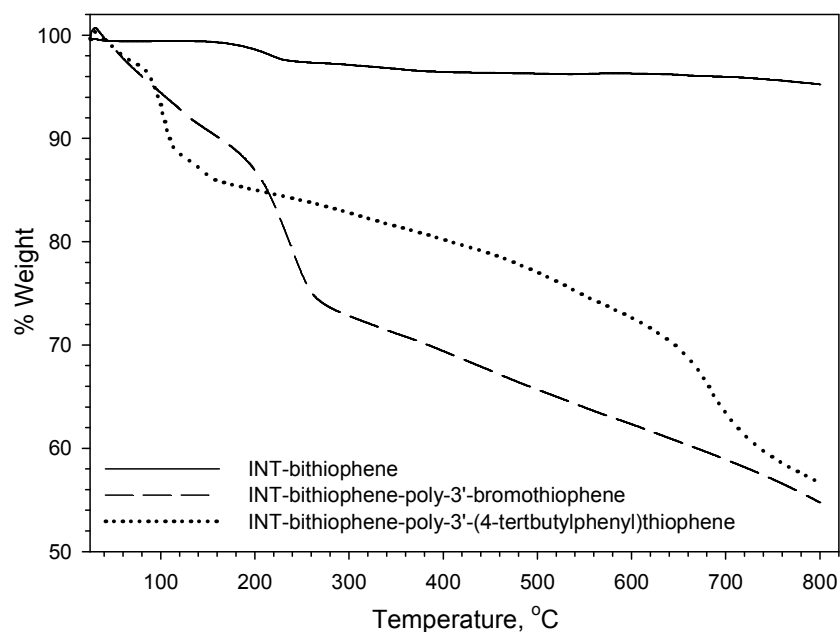
Figure 14 TGA spectra of the three mentioned composites *before* and *after* polymerization

In comparing both methods A and B (Scheme 6 and 7), method B delivered more organic material, which makes sense since 3'-(4-*tert* butyl-benzene) thiophene is a sterically hindered monomer that might interrupt/slower the

corresponding oxidative polymerization. In method B, one first polymerized the 3'-bromothiophene monomer followed by an effective Suzuki coupling to readily afford such a new hybrid functional polythiophene polymer. With this last method, one seriously improved the overall functionalization sequence yield since steric hinfrance plays a minimized role.

Stability test of coatings

In order to obtain such coating stability data, INTs-WS$_2$-bithiophene was first reacted with both aqueous 0.01M HCl and NH$_4$OH to determine both coating stabilities in acidic and basic media. This stability test was run and checked after one day, two days, and one week of media contacts. TGA analysis was then performed to calculate how much organic material was removed due to these acidic and basic conditions. TGA analysis (Figure 10) was also similarly performed to determine whether the INTs-WS$_2$-linker remained stable under acidic conditions.
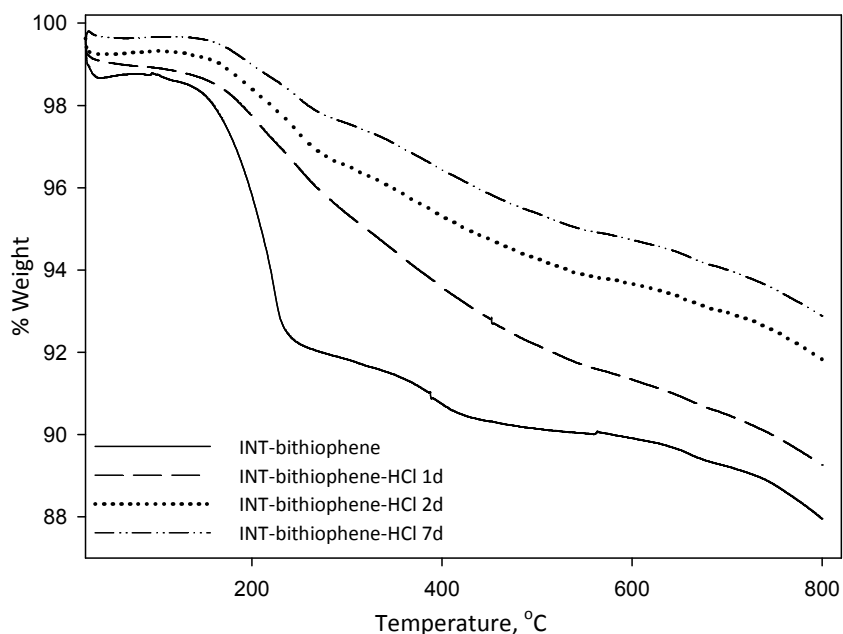

Figure 15 TGA spectra of INTs-WS$_2$-bithiophene after 0.01M HCl treatment (various contact times)

The TGA results indicate that part of this organic linker has been cleaved. After one day of 0.01M HCl treatment, 1.3 % of the organic material/linker have been removed, whereas after two days, 3.9% of this same linker have been removed. After one week, a 5.0% weight loss has been measured.
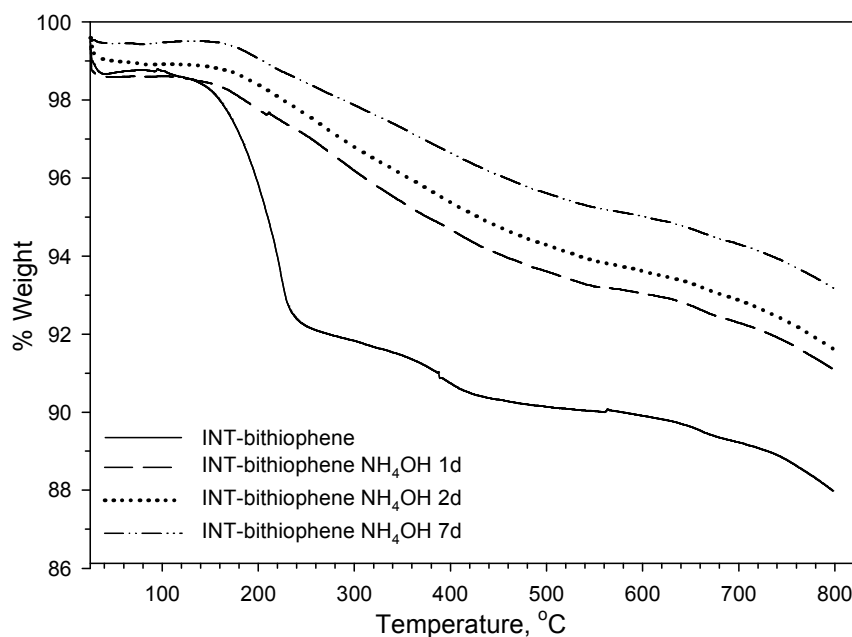
Figure 16 TGA spectra of INTs-WS$_2$-bithiophene after 0.01M NH$_4$OH treatment (various contact times)

The INTs-WS$_2$-bithiophene linker composite was also treated with 0.01M NH$_4$OH as well and the coating stability was TGA-tested after one day, two days, and one week. The TGA analysis shows very clearly that also basic conditions can cleave the bithiophene linker. One day of basic treatment caused the release of 3.15% of organic material, whereas after two days, 3.65%, and after one week, 5.24% of this same organic material. These results show that both acidic and basic conditions can cause cleavage of the bithiophene linker.

The ^{1}H-NMR of the obtained product from the filtrate exhibits peaks at 5.36 ppm 1H, 6.008ppm 1H, and 6.65ppm 1H. These peaks refer to the bithiophene unit (which protons? Precise) and confirm the observed linker cleavage.

$$\text{INTs/IFs WS}_2\text{-PTAA} \quad \xrightarrow{\text{HCl 0.01M}} \quad \text{INTs/IFs WS}_2 + \text{PTAA}$$
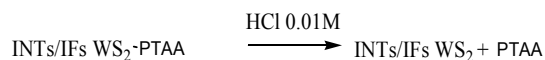
Scheme 8 Cleavage of INTs/IFs-WS$_2$-PTAA by 0.01M HCl

In order to determine the chemical stability of the tungsten disulfide-polymer composite under acidic conditions, both IFs and INTs WS$_2$-PTAA composites were stirred in 0.01M HCl for one day, two days, and one week. Both filtrate and WS$_2$ nanoparticles/nanotubes phases were then separated by centrifugation for charcaterization needs.

According to corresponding TGA spectra (Figure 17), aqueous 0.01M HCl is chemically reactive enough to cleave the polymeric PTAA phase from the nanomaterial surface. If the reaction takes longer, more PTAA is cleaved (4.0% after one day and 6.0% after two days). Thus, we can deduce that even at a low concentration of HCl (0.01M), the polymeric coating might be cleaved, which phenomenon can be very useful for drug delivery systems, for example.
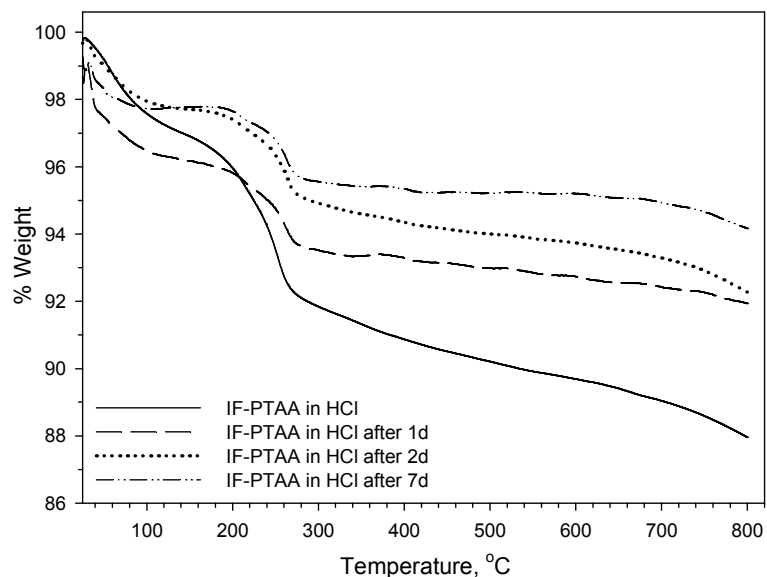
Figure 17 TGA spectra of IFs-WS$_2$-PTAA before and after HCl treatment (various contact times)

In addition, according to the TGA spectra (Figure 18) of INTs-WS$_2$-PTAA after one day of 0.01M HCl treatment, all the PTAA was cleaved (2.6% of organic material was left). Compared with the fullerene-PTAA composite, the nanotube-PTAA composite is less stable at high temperatures, which is reasonable due to the increased nanotube surface, which facilitate surface-localized reactions and phase/linker/chemical species cleavage.
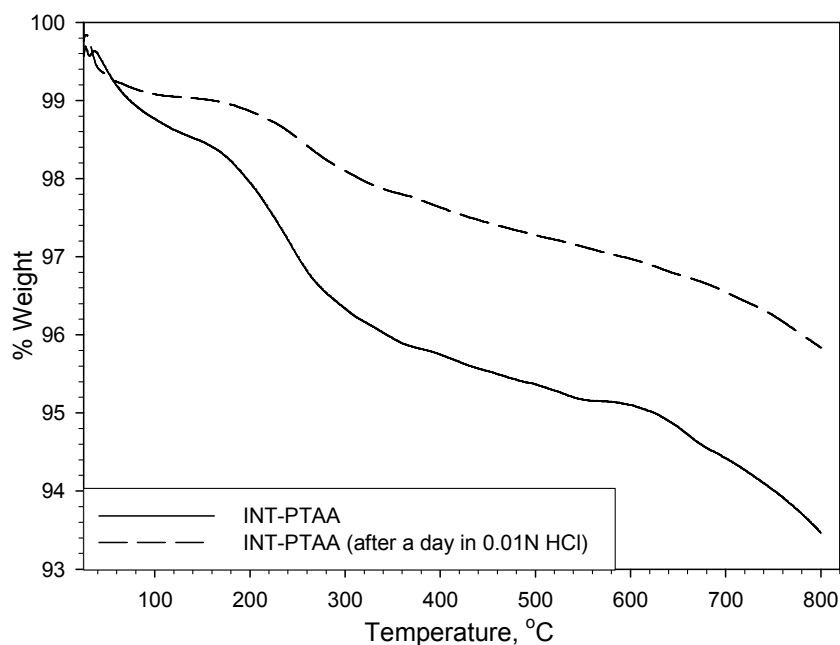

Figure 18 TGA spectra of INTs-WS$_2$-PTAA *before* and *after* HCl treatment

Moreover, Kaiser Tests dealing with INTs/IFs WS$_2$ PTAA composites following the HCl treatment (Table 4), showed that if the reaction takes longer, fewer carboxylic acid groups remain chemically accessible/reactive on the WS$_2$ nanomaterial surface.

Material	Kaiser Values
INTs-PTAA	0.2368 mmol/g
INTs-PTAA 1day HCl	0.0152 mmol/g
INTs-PTAA 2days HCl	0.014 mmol/g
IFs-PTAA	0.4553 mmol/g
IFs-PTAA 1day HCl	0.2269 mmol/g
IFs-PTAA 2days HCl	0.1629 mmol/g

Table 2 Kaiser Test *before* and *after* 0.01M HCl treatment

We can deduce from the Kaiser test results that the IFs-WS$_2$-PTAA composite contains more TAA units compared with INTs-WS$_2$-PTAA, which means that IFs-WS$_2$ are more surface-reactive than similar transition metal dichalcogenide INTs-WS$_2$.

Conclusions

A novel method for polymerization-driven surface functionalization (polythiophene acetic acid shell using a "growth from surface" concept) of INTs/IFs-WS$_2$ *via* an electrophilic reactive modified Vilsmeier–Haack-like reagent is described. This functional polymer shell can serve as an anchoring shell for subsequent second-step attachment of a wide variety of organic molecules, including other nanoscale components such as NPs, for example, onto the nanotube/fullerene surface using versatile, simple organic chemistry (EDC activation of polyCOOH), enabling surface property tuning to match charge, hydrophobicity/hydrophilicity, chemical functionality properties of any contacting material. In addition, the polymer coating may improve the mechanical properties of INTs/IFs. Since polythiophene derivatives are also electro-conductive components, they may seriously improve the overall electro-conductivity of corresponding nanotubes/fullerenes-based composite nanomaterials. In addition, such biocompatible polythiophene polymeric shells can be readily used as novel drug delivery systems that might be monitored (drug release control) under various acidic and/or basic conditions.

Acknowledgments

References

1.   Hussain ST, Abbas F, Kausar A, Khan MR. New polyaniline/polypyrrole/polythiophene and functionalized multiwalled carbon nanotube-based nanocomposites: Layer-by-layer in situ polymerization. High Perform Polym. 2013 February 1, 2013;25(1):70-8.

2.   Hanlon D, Backes C, Higgins TM, Hughes M, O'Neill A, King P, et al. Production of Molybdenum Trioxide Nanosheets by Liquid Exfoliation and Their Application in High-Performance Supercapacitors. Chem Mater. 2014;26(4):1751-63.

3.   Liu Y, Wang W, Huang H, Gu L, Wang Y, Peng X. The highly enhanced performance of lamellar WS 2 nanosheet electrodes upon intercalation of single-walled carbon nanotubes for supercapacitors and lithium ions batteries. Chem Commun. 2014;50(34):4485-8.

4.   Yuan Y, Li R, Liu Z. Establishing water-soluble layered ws2 nanosheet as a platform for biosensing. Anal Chem. 2014;86(7):3610-5.

5.   Rajesh, Ahuja T, Kumar D. Recent progress in the development of nano-structured conducting polymers/nanocomposites for sensor applications. Sensors and Actuators B: Chemical. 2009 2/2/;136(1):275-86.

6.   Ghose S, Watson KA, Delozier DM, Working DC, Siochi EJ, Connell JW. Incorporation of multi-walled carbon nanotubes into high temperature resin using dry mixing techniques. Composites Part A: Applied Science and Manufacturing. 2006 3//;37(3):465-75.

7.   Baibarac M, Gomez-Romero P, Lira-Cantú M, Casañ-Pastor N, Mestres N, Lefrant S. Electrosynthesis of the poly (N-vinyl carbazole)/carbon nanotubes composite for applications in the supercapacitors field. Eur Polym J. 2006;42(10):2302-12.

8.   Lee Y-K, Lee K-J, Kim D-S, Lee D-J, Kim J-Y. Polypyrrole-carbon nanotube composite films synthesized through gas-phase polymerization. Synth Met. 2010;160(7):814-8.

9.   Karim MR, Lee CJ, Lee MS. Synthesis and characterization of conducting polythiophene/carbon nanotubes composites. J Polym Sci, Part A: Polym Chem. 2006;44(18):5283-90.

10.   Song K, Zhang Y, Meng J, Green EC, Tajaddod N, Li H, et al. Structural polymer-based carbon nanotube composite fibers: understanding the processing–structure–performance relationship. Materials. 2013;6(6):2543-77.

11.   Kamiyama M, Soeda T, Nagajima S, Tanaka K. Development and application of high-strength polyester nanofibers. Polym J. 2012;44(10):987-94.

12.   Zhu F, Xin Q, Feng Q, Zhou Y, Liu R. Novel poly (vinylidene fluoride)/thermoplastic polyester elastomer composite membrane prepared by the electrospinning of nanofibers onto a dense membrane substrate for protective textiles. J Appl Polym Sci. 2015;132(26).

13.   Iijima S. Helical microtubules of graphitic carbon. nature. 1991;354(6348):56-8.

14.   Iijima S, Ichihashi T. Single-shell carbon nanotubes of 1-nm diameter. 1993.

15.   Salvetat J-P, Bonard J-M, Thomson N, Kulik A, Forro L, Benoit W, et al. Mechanical properties of carbon nanotubes. Appl Phys A. 1999;69(3):255-60.

16.   Tombler TW, Zhou C, Alexseyev L, Kong J, Dai H, Liu L, et al. Reversible electromechanical characteristics of carbon nanotubes under local-probe manipulation. Nature. 2000;405(6788):769-72.

17.   Treacy MJ, Ebbesen T, Gibson J. Exceptionally high Young's modulus observed for individual carbon nanotubes. 1996.

18.   Yu M-F, Lourie O, Dyer MJ, Moloni K, Kelly TF, Ruoff RS. Strength and breaking mechanism of multiwalled carbon nanotubes under tensile load. Science. 2000;287(5453):637-40.

19.   Yu M-F, Files BS, Arepalli S, Ruoff RS. Tensile loading of ropes of single wall carbon nanotubes and their mechanical properties. Phys Rev Lett. 2000;84(24):5552.

20.   Wong EW, Sheehan PE, Lieber CM. Nanobeam mechanics: elasticity, strength, and toughness of nanorods and nanotubes. Science. 1997;277(5334):1971-5.

21.   Peng B, Locascio M, Zapol P, Li S, Mielke SL, Schatz GC, et al. Measurements of near-ultimate strength for multiwalled carbon nanotubes and irradiation-induced crosslinking improvements. Nature nanotechnology. 2008;3(10):626-31.

22.   Demczyk B, Wang Y, Cumings J, Hetman M, Han W, Zettl A, et al. Direct mechanical measurement of the tensile strength and elastic modulus of multiwalled carbon nanotubes. Microsc Microanal. 2006;12(S02):934-5.

23.   Min BG, Chae HG, Minus ML, Kumar S. Polymer/carbon nanotube composite fibers—an overview. Functional Composites of Carbon Nanotubes and Applications. 2009;2:43-73.

24.   Coleman JN, Khan U, Blau WJ, Gun'ko YK. Small but strong: a review of the mechanical properties of carbon nanotube–polymer composites. Carbon. 2006;44(9):1624-52.

25.   Dondero WE, Gorga RE. Morphological and mechanical properties of carbon nanotube/polymer composites via melt compounding. J Polym Sci, Part B: Polym Phys. 2006;44(5):864-78.

26.   Khan U, Ryan K, Blau WJ, Coleman JN. The effect of solvent choice on the mechanical properties of carbon nanotube–polymer composites. Compos Sci Technol. 2007;67(15):3158-67.

27. Coleman JN, Cadek M, Ryan KP, Fonseca A, Nagy JB, Blau WJ, et al. Reinforcement of polymers with carbon nanotubes. The role of an ordered polymer interfacial region. Experiment and modeling. Polymer. 2006;47(26):8556-61.

28. Andrews R, Weisenberger M. Carbon nanotube polymer composites. Curr Opin Solid State Mater Sci. 2004;8(1):31-7.

29. Qian H, Greenhalgh ES, Shaffer MS, Bismarck A. Carbon nanotube-based hierarchical composites: a review. J Mater Chem. 2010;20(23):4751-62.

30. Tapeinos IG, Miaris A, Mitschang P, Alexopoulos ND. Carbon nanotube-based polymer composites: A trade-off between manufacturing cost and mechanical performance. Compos Sci Technol. 2012 4/13/;72(7):774-87.

31. Lalwani G, Henslee AM, Farshid B, Parmar P, Lin L, Qin Y-X, et al. Tungsten disulfide nanotubes reinforced biodegradable polymers for bone tissue engineering. Acta biomaterialia. 2013;9(9):8365-73.

32. Zohar E, Baruch S, Shneider M, Dodiuk H, Kenig S, Tenne R, et al. The Effect of WS2 Nanotubes on the Properties of Epoxy-Based Nanocomposites. J Adhes Sci Technol. 2011 2011/01/01;25(13):1603-17.

33. Reddy CS, Zak A, Zussman E. WS 2 nanotubes embedded in PMMA nanofibers as energy absorptive material. J Mater Chem. 2011;21(40):16086-93.

34. Kaplan-Ashiri I, Cohen SR, Gartsman K, Ivanovskaya V, Heine T, Seifert G, et al. On the mechanical behavior of WS2 nanotubes under axial tension and compression. Proceedings of the National Academy of Sciences of the United States of America. 2006;103(3):523-8.

35. Rozenberg B, Tenne R. Polymer-assisted fabrication of nanoparticles and nanocomposites. Prog Polym Sci. 2008;33(1):40-112.

36. Binyamini RBS, Boguslavsky Y, Laux E, Keppner H, Lellouche J-PM. A simple one-step approach to the decoration of parylene C coatings using functional silica-based NPs. Surf Coat Technol. 2015 2/15/;263(0):36-43.

37. Raichman D, Strawser D, Lellouche J-P. Covalent functionalization/polycarboxylation of tungsten disulfide inorganic nanotubes (INTs-WS2). Nano Res. 2015 2015/05/01;8(5):1454-63. English.

38. Simonyan MA, Dib K, Pashkov AN, Simonyan AV, Myachina OV, Ostrovskii OV. Synthesis and antiradical and antioxidant activity of cycvalon and its analogs. Pharm Chem J. 2007 2007/08/01;41(8):403-6. English.